# SUPERSONIC MINIMUM LENGTH NOZZLE DESIGN FOR DENSE GASES

Andrew C. Aldo* and Brian M. Argrow**
Department of Aerospace Engineering Sciences
University of Colorado
Boulder, Colorado 80309

## ABSTRACT

Recently, dense gases have been investigated for many engineering applications such as for turbomachinery and wind tunnels. Supersonic nozzle design for these gases is complicated by their nonclassical behavior in the transonic flow regime. In this paper a method of characteristics (MOC) is developed for two-dimensional (planar) and, primarily, axisymmetric flow of a van der Waals gas. Using a straight sonic line assumption, a centered expansion is used to generate an inviscid wall contour of minimum length. The van der Waals results are compared to previous perfect gas results to show the real gas effects on the flow properties and inviscid wall contours.

## INTRODUCTION

A minimum length nozzle (MLN) produces a uniform supersonic flow with a minimum ratio of throat height or radius to total nozzle length. Argrow and Emanuel (refs. 1, 2) present detailed discussion of MLN designs, comparisons of different types, computational flow field analysis, and engineering applications. Until this paper, all MLN analyses, that we are aware of, have focused only on perfect gas results. Several authors (refs. 3–10) have recently investigated nozzle flows for nonideal gases. References 3–5 and 8–11 discuss steady flows of dense gases. Cramer (ref. 11) refers to these gases as BZT (Bethe-Zel'dovich-Thompson) to recognize the individuals that first theorized their nonclassical behavior. Such behavior includes local a minimum of the Mach number during steady isentropic expansion, expansion shocks, increase in the critical Mach number, and other nonclassical behaviors. BZT fluids typically have large polyatomic molecules with comparatively large specific heats.

All the previously mentioned references that investigate BZT fluids discuss the thermodynamic condition that governs the classical or nonclassical behavior. The governing thermodynamic parameter is

$$\Gamma = 1 + \frac{\bar{\varrho}}{\bar{a}}\left(\frac{\partial \bar{a}}{\partial \bar{\varrho}}\right)_{\bar{s}}$$

where

$$\bar{a} = \left(\frac{\partial \bar{p}}{\partial \bar{\varrho}}\right)_{\bar{s}}^{1/2}$$

is the speed of sound, $\bar{\varrho}$, $\bar{p}$, and $\bar{s}$ are the density, pressure, and entropy, respectively. The overbar indicates dimensional quantities. The parameter $\Gamma$ is referred to by Thompson (ref. 13) as the fundamental derivative of gas dynamics.

For most fluids $\Gamma > 0$ under normal conditions, but for BZT fluids may have $\Gamma < 0$. The $\Gamma < 0$ region of a BZT gas (dense gas) occurs in the dense gas region near the saturated vapor curve in the $pv$ plane. Practical uses for the nonclassical behavior of BZT fluids include turbomachinery and heavy-gas

*Graduate Student
**Assistant Professor

wind tunnels. Discussion of the various applications that may capitalize on the nonclassical behavior of BZT fluids can be found in refs. 3, 5, and 8–12.

The most apparent application of a MLN designed for dense-gas flow is for heavy-gas wind tunnels. Anderson (ref. 9) shows Navier–Stokes calculations for the flow of sulfur hexaflouride ($HF_6$) over a NACA 0012 airfoil. This study investigated the feasibility of using this large-molecule gas for wind tunnel applications. While most of the previous references speculate that nozzles can be designed to produce supersonic flow of a BZT fluid, the calculations have been limited to one-dimensional cases (refs. 3–5, 8, 10, 11).

## THERMODYNAMIC MODEL

The van der Waals equation of state is

$$\bar{p} = \frac{\overline{R}\overline{T}}{\bar{v} - \bar{b}} - \frac{\bar{a}}{\bar{v}^2},$$

where $\overline{R}$ is the specific gas constant, $\bar{v}$ is the specific volume, and

$$\bar{b} = \frac{\overline{R}\overline{T}_c}{8\bar{p}_c} \quad \text{and} \quad \bar{a} = \frac{27}{64}\frac{\overline{R}^2\overline{T}_c^2}{\bar{p}_c}.$$

The $c$ subscript refers to conditions at the critical point. The following thermodynamic development and nondimensionalization scheme follows that of ref. 12. The enthalpy $\bar{h}$ and speed of sound $\bar{a}$ are given by

$$\bar{h} = \bar{e}_r + \frac{\overline{R}\overline{T}}{\delta}\left(1 + \delta\frac{\bar{v}}{\bar{v} - \bar{b}}\right) - \frac{2\bar{a}}{\bar{v}},$$

$$\bar{a} = \left[\left(\frac{\bar{v}}{\bar{v} - \bar{b}}\right)^2 \overline{R}\overline{T}(1 + \delta) - \frac{2\bar{a}}{\bar{v}}\right]^{1/2},$$

Here $\bar{e}_r$ is an arbitrary reference energy and

$$\delta \equiv \overline{R}/\bar{c}_v$$

Because there is minimal temperature variation for the flows investigated, we assume a constant $\bar{c}_v = \bar{c}_{v\,\infty}$, where $\bar{c}_{v\,\infty}$ is the ideal gas specific heat. The temperature variation for isentropic flow of a van der Waals gas is given by

$$\frac{\overline{T}}{\overline{T}_0} = \left(\frac{\bar{v}_0 - \bar{b}}{\bar{v} - \bar{b}}\right)^{\delta},$$

where the 0 subscript refers to stagnation conditions.

The nondimensional (reduced variable) form of the van der Waals equation is written as

$$p = \frac{8T}{3v - 1} - \frac{3}{v^2},$$

and the critical compressibility is

$$Z_c = \left(\frac{pv}{RT}\right)_c = \frac{3}{8}$$

with the reduced variables

$$p = \frac{\bar{p}}{p_c}, \quad T = \frac{\bar{T}}{T_c}, \quad v = \frac{\bar{v}}{v_c}.$$

The nondimensional form of the other thermodynamics relations are

$$T = T_0\left(\frac{v_0 - b}{v - b}\right)^{\delta},$$

$$h = \frac{T}{\delta}\left(1 + \delta\frac{v_0}{v_0 - b}\right) - \frac{2a}{v_0},$$

$$a = \left[T(1 + \delta)\left(\frac{v}{v - b}\right)^2 - \frac{2a}{v}\right]^{1/2},$$

$$M = \frac{\sqrt{2(h_0 - h)}}{a},$$

where

$$h \equiv \frac{\bar{h} - \bar{e}_r}{\bar{R}T_c}, \quad a \equiv \frac{\bar{a}}{\sqrt{\bar{R}T_c}}, \quad b \equiv \frac{\bar{b}}{\bar{v}_c} = \frac{1}{8Z_c}, \quad a \equiv \frac{\bar{a}}{\bar{R}T_c\bar{v}_c} = \frac{27}{64}\frac{1}{Z_c}.$$

## METHOD OF CHARACTERISTICS FOR REAL GASES

The method of characteristics (MOC) used by Argrow and Emanuel (ref. 1) assumes an isentropic, irrotational flow of a perfect gas. For this case, the governing two–dimensional partial differential equation reduces to a set of four algebraic equations, two characteristic and two compatibility equations. For the axisymmetric case, the characteristic and compatibility equations form a set of four ordinary differential equations that are solved simultaneously. Details of the solution procedures can be found in ref. 1.

A MOC for the isentropic two–dimensional or axisymmetric flow of a real gas (ref. 14) is used for the present study. The method is completely general and we use the van der Waals thermodynamic model more for simplicity than for accuracy. The governing partial differential equations (PDEs) are given by the gas dynamic equation, the irrotationality condition, and the speed of sound relation,

$$(V_x^2 - a^2)V_x + (V_y^2 - a^2)V_y + 2V_xV_y\frac{\partial V_x}{\partial y} - \sigma\frac{a^2V_y}{y} = 0,$$

$$\frac{\partial V_x}{\partial y} - \frac{\partial V_y}{\partial x} = 0,$$

$$a = a(V) = a(V_x, V_y),$$

where $\sigma = 0$ for two-dimensional flow or $\sigma = 0$ for axisymmetric flow, $x$ and $y$ are the axial and radial (transverse) coordinates nondimensionalized with respect to throat radius or half-height, $V_x$ and $V_y$ are the corresponding velocity components, and $V$ is the velocity magnitude, all velocities are nondimensionalized in the same manner as the speed of sound $\bar{a}$. Along the characteristic lines, that correspond to Mach lines in the flow, this system of PDEs reduces to two ordinary differential equations called compatibility equations. Fig. 1 is a schematic of the supersonic flow field showing the MLN geometry and the flow geometry associated with an arbitrary point on a streamline. The angle $\theta^*$ is the initial inclination of the supersonic contour. The left and right running characteristics designated as $C_+$ and $C_-$ are Mach lines inclined at the Mach angle $\mu$ with respect to the velocity vector $V$. The corresponding characteristic and compatibility equations are

$$C_\pm \text{ characteristic equation}: \left(\frac{dy}{dx}\right)_\pm = \lambda_\pm = \tan(\theta \pm \mu), \tag{1a}$$

$$C_\pm \text{ compatibility equation}: (V_x^2 - a^2)dV_{x_\pm} + [2V_xV_y - (V_x^2 - a^2)\lambda_\pm]dV_{y_\pm} - \sigma\frac{a^2V_y}{y}dx_\pm = 0. \tag{1b}$$

The gas is assumed to enter the supersonic portion of the nozzle along the straight sonic line $OA$ uniform and parallel to the axis. It is then expanded and accelerated (or possibly decelerated in the $\Gamma < 0$ region) through the nozzle and exits the nozzle with a uniform flow crossing the terminating characteristic $BC$ at the exit Mach number $M_f$. For the two-dimensional nozzle, the centered expansion generated by the sharp throat is a Prandtl-Meyer expansion. In the axisymmetric case, the flow at the wall is locally two-dimensional, thus at the throat the expansion is locally Prandtl-Meyer. Construction of the flow field begins by discretizing the centered expansion into equally-spaced velocity increments. Each velocity increment $\Delta V$ has an associated isentropic flow turn angle increment $\Delta\theta$. The angle increment $\Delta\theta$ is computed from the relation

$$\theta_2 - \theta_1 = \int_{V_1}^{V_2} \frac{\sqrt{M^2 - 1}}{V} dV. \tag{2}$$

For a perfect gas, the $\Delta M$ associated with an angular deflection $\Delta\theta$ can be easily determined from the Prandtl-Meyer function. For a real gas, the Prandtl-Meyer computation requires the solution of a system of ordinary differential equations as shown by Cramer (ref. 10). We avoid the Prandtl-Meyer computation by using the angle-velocity relation, equation (2).

With the position of the throat specified and the velocity components $(V_x, V_y)$ computed from $V$ and $\theta$, the necessary independent variables are determined at the throat. Equations (1) are solved simultaneously using the second-order average-property Euler predictor-corrector scheme described in ref. 14. The characteristic net of the kernel region $OAB$ and the transition region $ABC$ is constructed using the unit processes described in ref. 1. The wall contour corresponds to the streamline that passes through points $A$ and $C$. This streamline is determined by also using the average-property Euler predictor-corrector scheme to integrate the equation

$$\frac{dy_w}{dx} = \tan\theta_w$$

from the initial condition, $\theta_w = \theta^*$ at $x = 0$ to the exit condition $\theta_w = 0$ at $x_f = 0$.

The accuracy of the characteristic computations and the wall contour are affected by the spacing of the characteristic nodes. The $C_-$ characteristics that emanate from the corner at point $A$ reflect from the axis as $C_+$ characteristics and bend away from the center of the expansion. This causes relatively large spacing between characteristic node points and the subsequent computed wall points just downstream of the throat where the gradients are largest. To alleviate this situation, the characteristic net is compressed toward the sonic line by decreasing the step size of the speed increments in the centered expansion discretization. The Prandtl–Meyer and turn angles in ref. 1 are discretized and compressed in a similar manner.

## RESULTS

For the nominal case of $T_0$ =1.01, $\delta$ = 0.02, and $\nu_0$ = 0.70, $dV \cong \delta V = 10^{-6}$ for equation (2). The first characteristic is chosen at $\delta V$, then the step size is increased until a characteristic is generated at every $20\delta V$. This allows characteristics to be compressed towards the sonic line for improved accuracy. For the nominal case, the limits of integration for equation (2) are set at the sonic speed $V_1 = 0.26$ to $V_2 = 0.9V_{max}$ with $V_{max} = 9.93$. Characteristic spacing in the transition region is controlled by an aspect ratio that keeps the shape of the characteristic cells as uniform as needed. For the relatively short nozzles produced in this study, the aspect ratio was set at 0.5. Reference 1 gives a complete description of how the characteristic compression and transition region aspect ratio affect the overall computational accuracy.

Figures 2 show the wall contour and the variation of $M$, $\varrho$, and $\Gamma$ along the axis and along the wall for a two–dimensional nozzle with $T_0$ =1.01, $\delta$ =0.02, and $\nu_0$ =0.70, 0.85. Figure 2(a) indicates the increase in nozzle length required for the more dense gas. Note that $\theta^*$ is fixed at 2.5° for the comparisons in Figs. 2. This is near the maximum value of $\theta^*$ where the $C_-$ characteristic, near $AB$ of Fig. 1, begin to overlap other $C_-$ characteristics in the kernel, or there is overlapping from $C_+$ characteristics near $BC$ with both instances producing an oblique expansion shock. Once a shock occurs (compression or expansion), the flow is no longer isentropic and the MOC cannot be applied without some special procedure to account for the placement of the shock (We do not to incorporate such a procedure in the MOC used for this study.)

For Figs. 2(b–d), the axis curves are terminated at the end of the kernel because the uniform flow region begins at point $B$ as shown in Fig. 1. The wall curves extend to the end of the contour at point $C$ as also shown in Fig. 1. The density $\varrho$ decreases smoothly along the axis and wall for both cases as shown in Fig. 2(b). Figure 2c shows that the gas is expanded into a $\Gamma < 0$ region that extends through the nozzle exit for the nominal $\nu_0$ =0.70 case. This produces a uniform supersonic flow with $\Gamma < 0$. For this case, the Mach number reaches a maximum of about 1.88 along the axis and along the wall, as shown in fig. 2d. This agrees with the quasi one–dimensional results obtained by Cramer and Best (ref. 12).

A comparison of the wall contours at the maximum $M_f$ for the two–dimensional and axisymmetric nominal cases is shown in Fig. 3. Note that in the contour plots, the $y$–axis is not to scale. Although difficult to see, the axisymmetric contour contains an inflection point just downstream of the throat that is not present in the two–dimensional contour. Also, $\theta^*$ is larger for the two–dimensional case as will be shown in more detail in the following figures. The results of this plot agree with the perfect gas results of Argrow and Emanuel (ref. 1).

Figures 4(a) and 4(b) show the $\theta^*$ vs. $M_f$ variation for the axisymmetric and two–dimensional cases, respectively. These figures show the nominal case, a perfect gas with nominal conditions, and nominal conditions with $\nu_0 = 0.85$. Varying stagnation conditions for the perfect gas does not effect the nondimensional results. The dense gas case, $\nu_0 = 0.7$, shows BZT gas behavior, reaching a maximum $M_f$ of about 1.88 for $\theta^*$ near 1° for the axisymmetric case shown in Fig 4(a). Then $M_f$ decreases until reaching a maximum $\theta^*$ value of about 2.5°. The maximum $M_f$ for the two–dimensional case is at $\theta^* \cong 2.5°$. The decrease of $M_f$ for $\theta^* > 2.5°$ is not shown in Fig. 4(b), although the maximum $\theta^*$ for this case is about 3.5°.

Figures 5 and 6 also show $\theta^*$ vs. $M_f$ for the for the nominal axisymmetric case. Figure 5 shows the effect of varying $T_0$, keeping other nominal conditions fixed, compared to a perfect gas. This shows that slightly increasing $T_0$ moves the flow away from the dense gas region. Figure 6 shows the effect of varying

$c_v/R$, keeping the other nominal conditions fixed, compared to a perfect gas. This shows a tendency to approach perfect gas behavior as $c_v/R$ is decreased.

Figures 7 and 8 show the variation of the kernel length $x_B$ and nozzle length $x_f$ vs. $M_f$, respectively. Note that for the two-dimensional case, the figures show the increase to the maximum lengths but the decrease as $\theta^*$ increases (and $M_f$ decreases from the maximum) is not shown in these plots. The BZT gas behavior is indicated in the nominal cases. Because the gas is more dense, the lengths are longer and reach a maximum before decreasing.

## CONCLUSIONS

The MOC is applied to the steady isentropic flow of a dense gas. A method is presented for generating inviscid MLN contours to produce a uniform supersonic flow. The MLN procedure presented is limited to cases where there is only one sonic point. Inclusion of more than one sonic point will require the coupling of the present method with a subsonic contour design procedure. In order to continuously isentropically expand the gas from a stagnation state to $M \to \infty$, reference 12 shows that for the nominal case investigated in the present study, $M$ first reaches a local maximum value of about 1.88 before decreasing to a supersonic minimum of about 1.05. We have shown that it is not possible for a nozzle to use a single centered expansion to accomplish this. At best, the single centered-expansion MLN can generate an isentropic expansion slightly beyond the local maximum before an expansion shock is generated. The maximum allowable $\theta^*$ appears to occur as the $\Gamma < 0$ region approaches the throat, resulting in a shock. We speculate that a design that employs two centered expansions separated by a finite converging wall may be able to accomplish the expansion in a minimum length. This will be investigated in the future.

It was shown that the nozzle designs presented may be used to produce a steady supersonic flow of a BZT gas in a $\Gamma < 0$ state. This raises the possibility of producing interesting wind tunnel experiments to study the supersonic external flow of a dense gas over airfoils and other aerodynamic shapes.

## ACKNOWLEDGEMENT

The authors gratefully acknowledge Mark. S. Cramer and George Emanuel for their insightful correspondence and suggestions.

## REFERENCES

1. Argrow, B. M. and Emanuel, G., "Comparison of Minimum Length Nozzles," J. of Fluids Engineering
2. Argrow, B. M.; and Emanuel, G.: Computational Analysis of the Transonic Flow Field of Two-Dimensional Minimum Length Nozzles. J. Fluids Eng., vol. 113, Sept. 1991, pp. 479-488.
3. Cramer, M. S.; and Fry, R. N.: Nozzle Flows of Dense Gases. Phys. Fluids A, vol. 5, May 1993, pp. 1246-1259.
4. Chandrasekar, D.; and Prasad, P. P.: Transonic Flow of a Fluid with Positive and Negative Nonlinearity through a Nozzle. Phys. Fluids A., vol. 3, Mar. 1991, pp. 427-438.
5. Schnerr, G. H.; and Leidner, P.: Diabatic Supersonic Flows of Dense Gases. Phys. Fluids A, vol. 3, Oct. 1991, pp. 2445- 2458.
6. Bober, W.; and Chow, W. L.: Nonideal Isentropic Gas Flow Through Converging-Diverging Nozzles. J. Fluids Eng., vol. 112, Dec. 1990, pp 455-460.
7. Vinokur, M.: Discussion of Nonideal Isentropic Gas Flow Through Converging-Diverging Nozzles. J. Fluids Eng., vol. 112, Dec. 1990, pp. 460-461.
8. Kluwick, A.: Transonic Nozzle Flow of Dense Gases. J. Fluid Mech., vol. 247, 1993, pp. 661-688.
9. Anderson, W. K.: Numerical Study on Using Sulfur Hexaflouride as a Wind Tunnel Test Gas. AIAA J., vol. 29, Dec. 1991, pp. 2179-2180.
10. Cramer, M. S.; and Crickenberger, A. B.: Prandtl-Meyer Function for Dense Gases. AIAA J., vol. 30, Feb. 1992, pp. 561-564.

11. Cramer, M. S.: Nonclassical Dynamics of Classical Gases. Nonlinear Waves in Real Fluids, Springer-Verlag, 1991, pp. 91-145.
12. Cramer, M. S.; and Best, L. M.: Steady, Isentropic Flows of Dense Gases. Phys. Fluids A, vol. 3, Jan. 1991, pp. 219-226.
13. Thompson, P. A.: A Fundamental Derivative in Gasdynamics. Phys. Fluids, vol. 14, 1971, pp. 1843-1849.
14. Zucrow, M. J.; and Hoffman Gas Dynamics. Vol. 1. Wiley, 1976, vol. 2 Krieger, 1977.

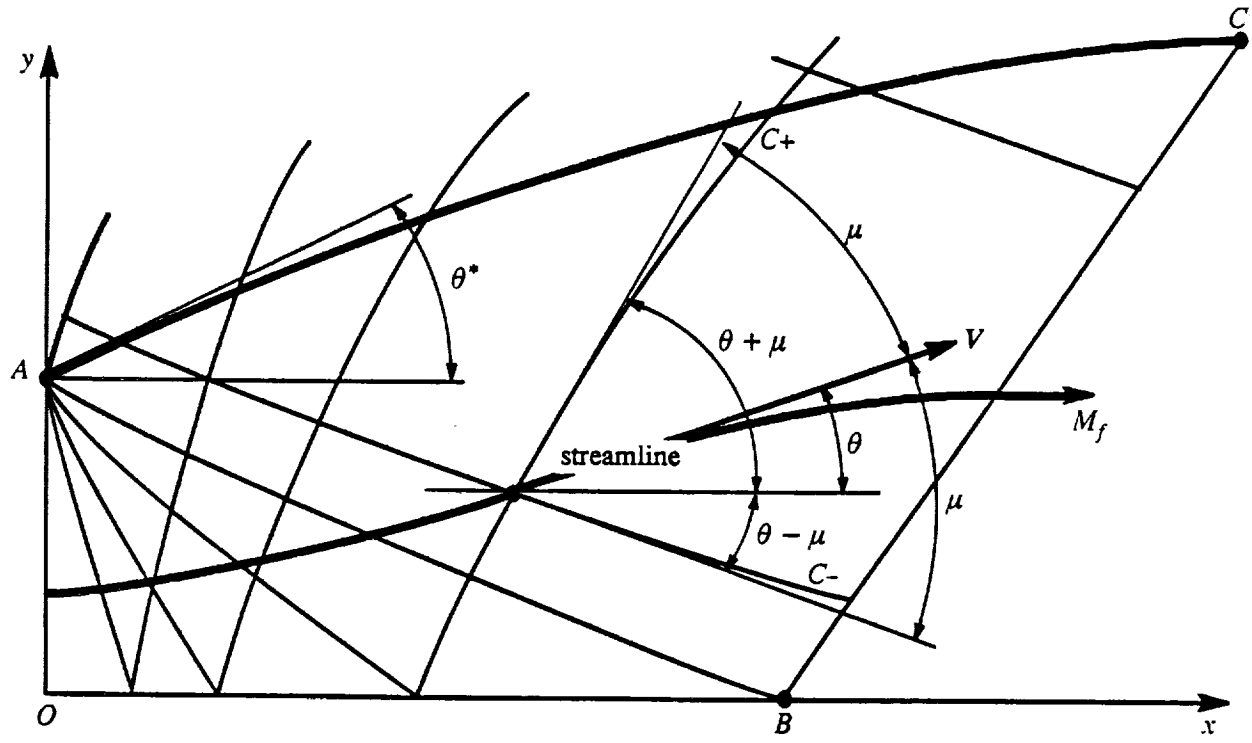


**Fig. 1** MLN supersonic flow field geometry, upper half-plane.

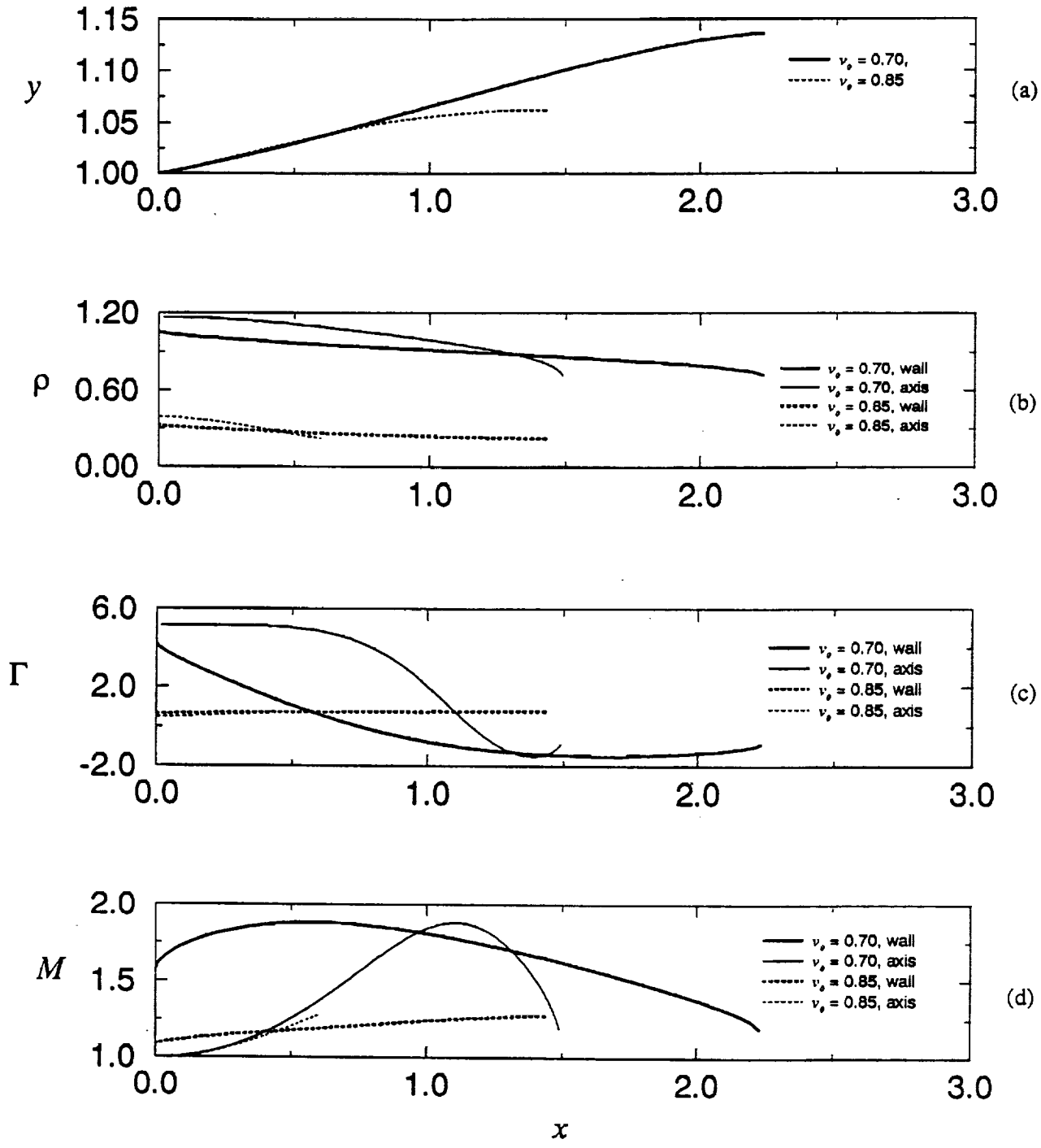


**Fig. 2** (a) Wall contour, (b) density, $\varrho$, distributions (c) fundamental derivative, $\Gamma$, distributions; (d) Mach number, $M$, distributions, along the wall and the axis, all for the axisymmetric case, nominal and for $v_0 = 0.85$.

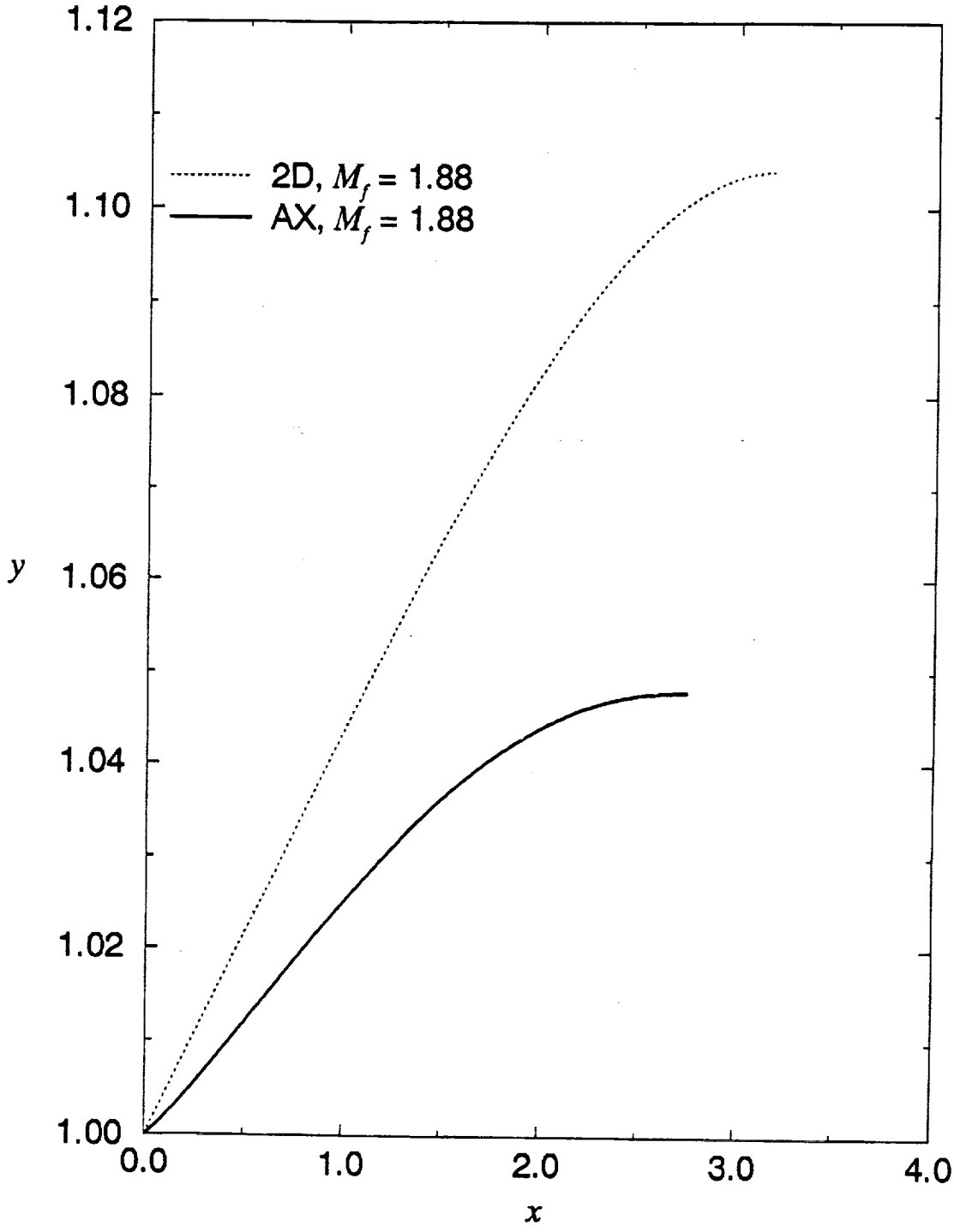


**Fig. 3** Comparison of two-dimensional and axisymmetric contours for maximum $M_f$, nominal case.

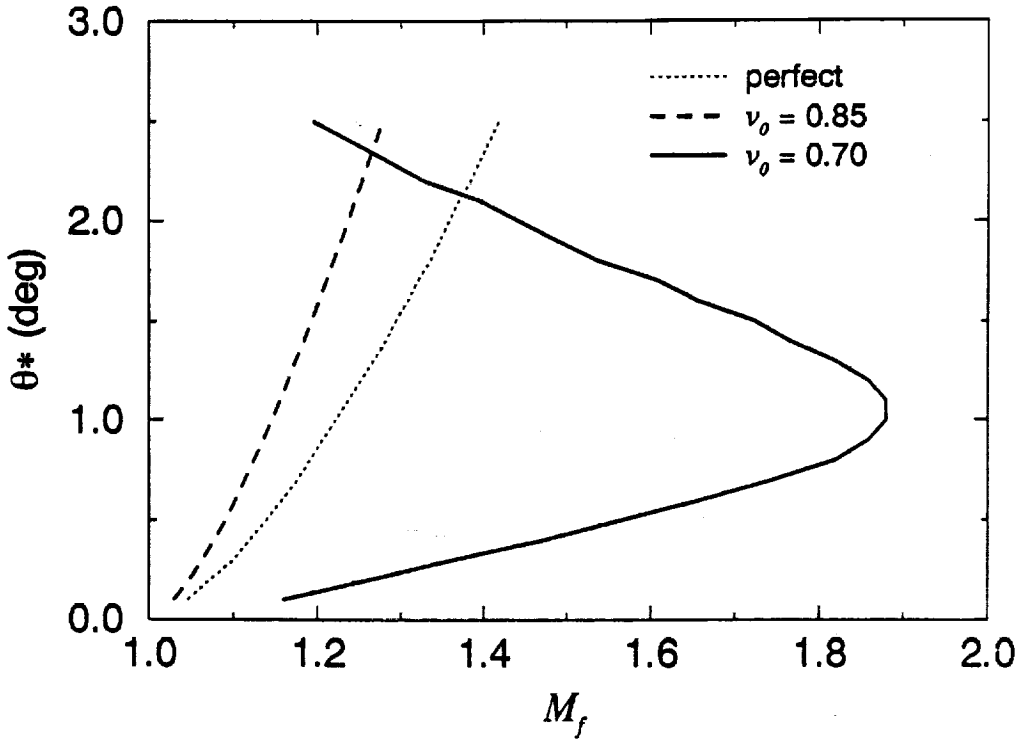


**Fig. 4** (a) Initial wall turn angle $\theta^*$ vs. $M_f$, nominal conditions, variable $\nu_0$, axisymmetric case.

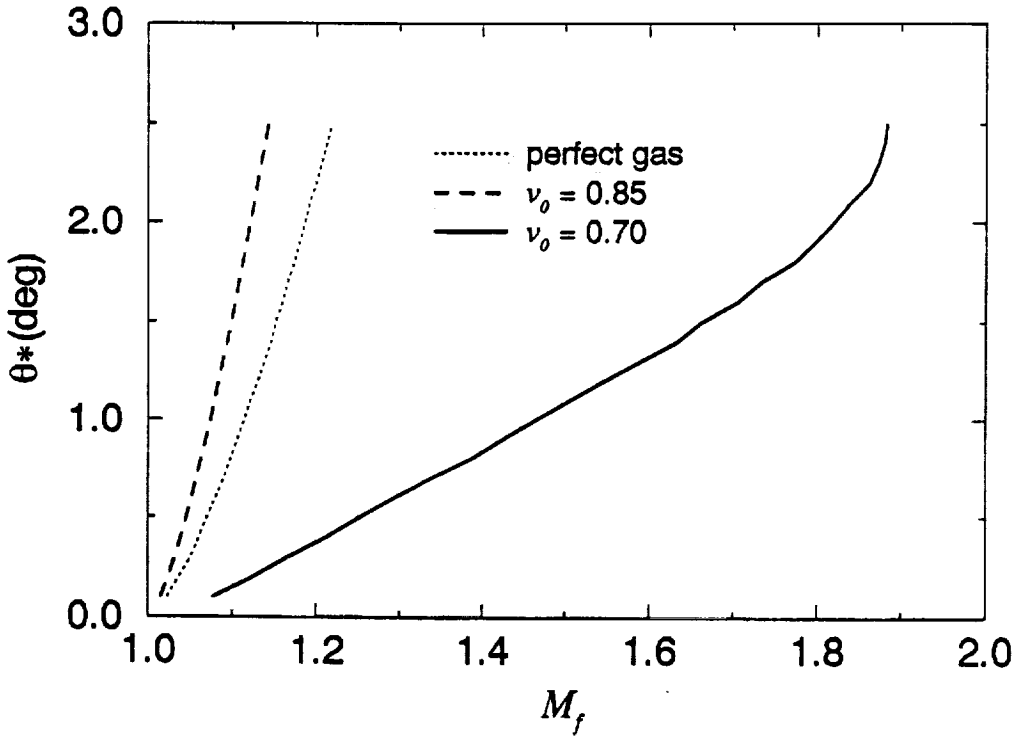


**Fig. 4** (b) Initial wall turn angle $\theta^*$ vs. $M_f$, nominal conditions, variable $\nu_0$, two-dimensional case.

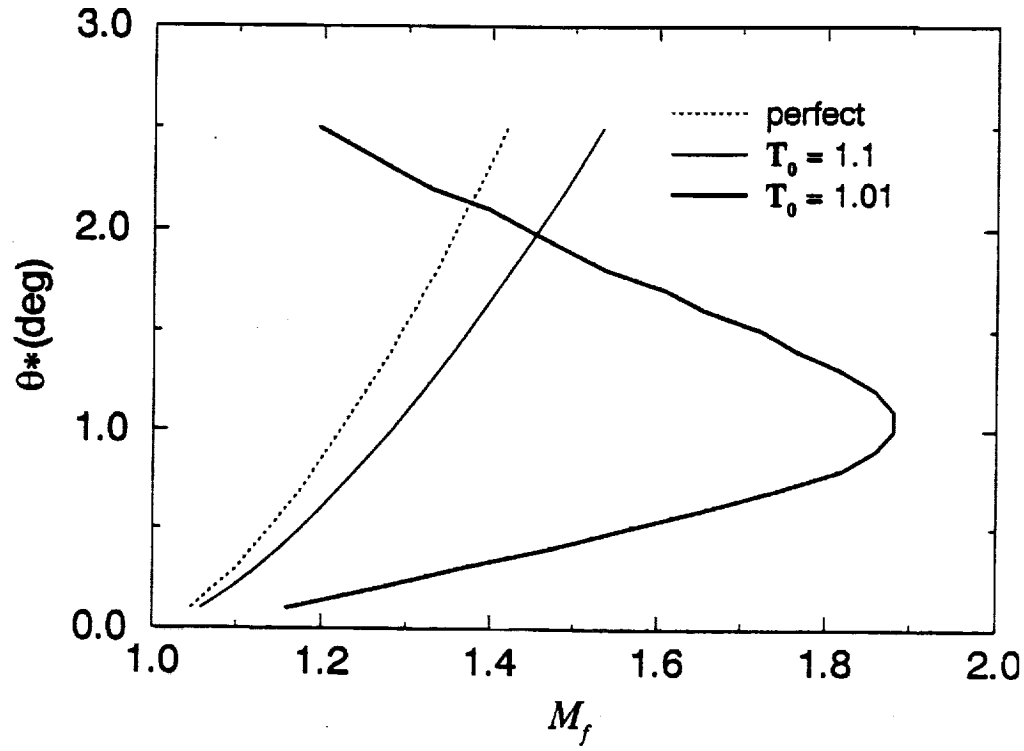


**Fig. 5** Initial wall turn angle $\theta^*$ vs. $M_f$, nominal conditions, variable $T_0$, axisymmetric case.

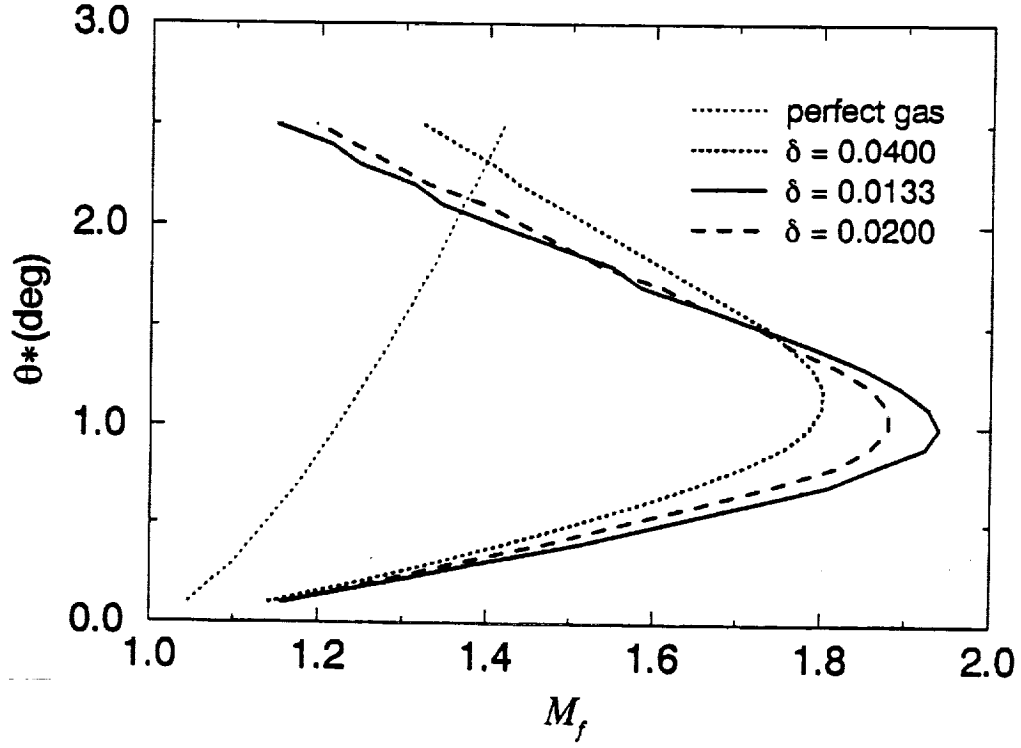


**Fig. 6** Initial wall turn angle $\theta^*$ vs. $M_f$, nominal conditions, variable $c_v/R$, axisymmetric case.

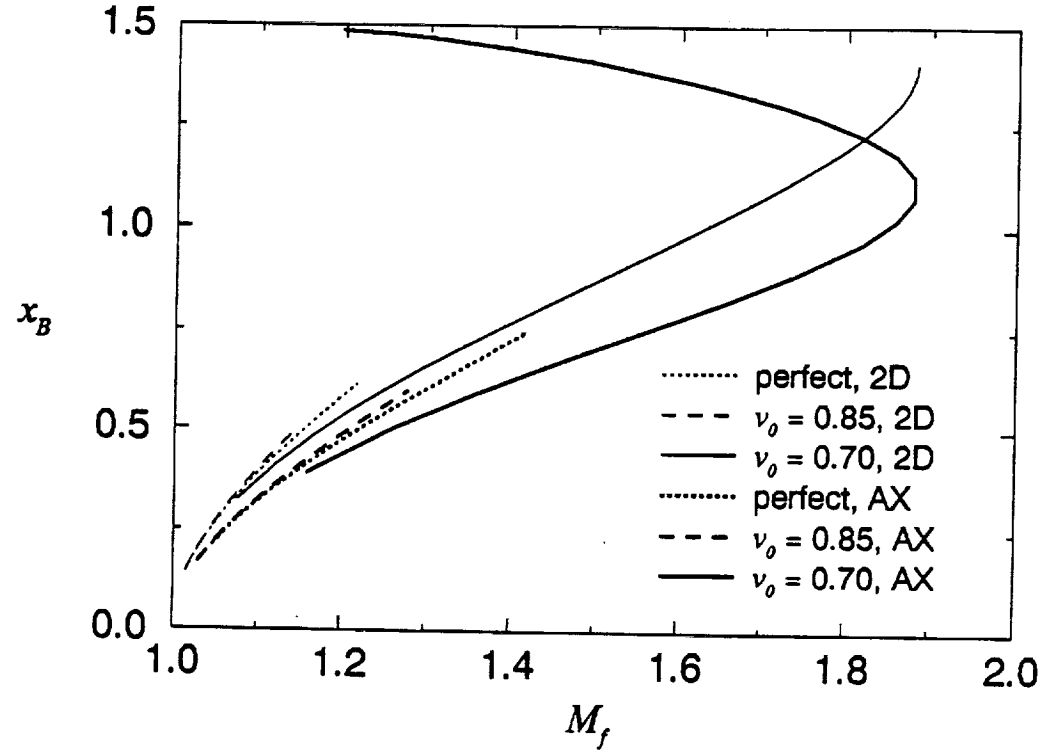


**Fig. 7** Kernel length $x_B$ vs. $M_f$, nominal two-dimensional and axisymmetric cases with variable $\nu_0$.

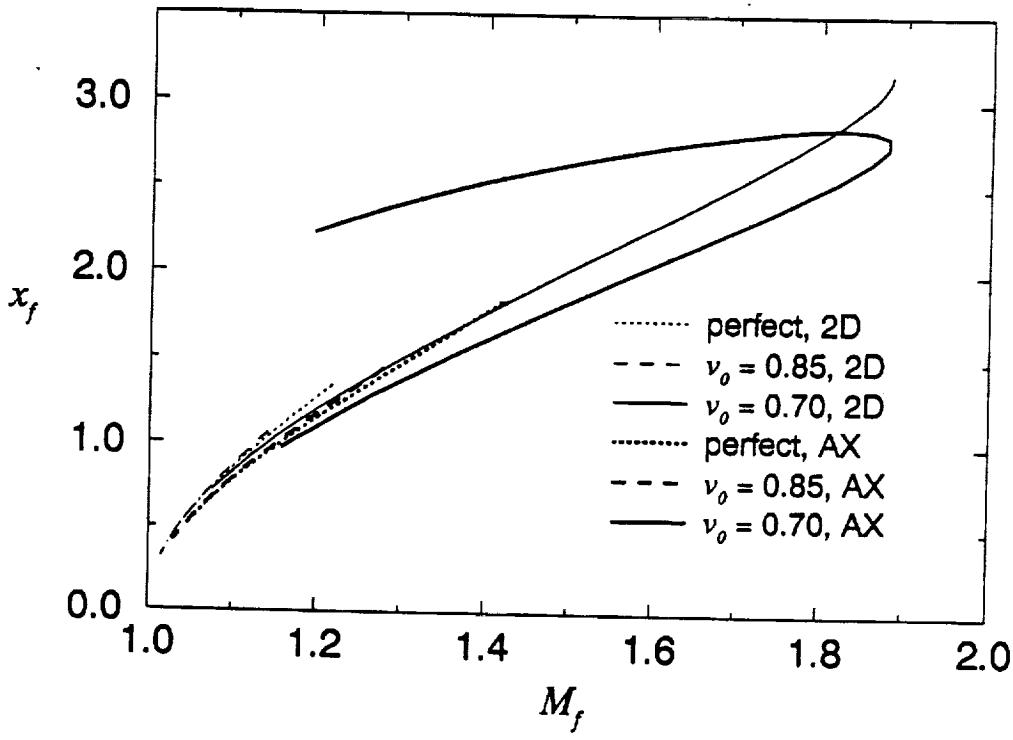


**Fig. 8** Nozzle length $x_f$ vs. $M_f$, nominal two-dimensional and axisymmetric cases with variable $\nu_0$.